is seen for the more viscous fluid which lags behind the displacement front. Here, the most prolate drops lag the farthest behind the front.

LITERATURE CITED

1. P. G. Saffman and G. Taylor, "The penetration of a fluid into a porous medium or Hele–Shaw cell containing a more viscous fluid," Proc. R. Soc., 245A, No. 1242 (1958).
2. Sir Geoffrey Taylor and P. G. Saffman, "A note on the motion of bubbles in a Hele–Shaw cell and porous medium," Q. J. Appl. Mech. Math., XII, Pt. 3, No. 8 (1959).
3. P. G. Saffman, "Viscous fingering in Hele–Shaw cells," J. Fluid Mech., 173, No. 12 (1986).
4. G. Tryggvason and H. Aref, "Numerical experiments on Hele–Shaw flow with a sharp interface," ibid., 136, No. 11 (1983).
5. G. Tryggvason and H. Aref, "Finger-interaction mechanisms in stratified Hele–Shaw flow," ibid., 154, No. 5 (1985).
6. Oe. Madelung, Mathematical Physics [Russian translation], Nauka, Moscow (1968).
7. T. Maxworthy, "Bubble formation, motion, and interaction in Hele–Shaw cell," J. Fluid Mech., 173, No. 12 (1986).

NONSTEADY THERMAL CONVECTION IN A HORIZONTAL CYLINDER WITH A NONUNIFORM DISTRIBUTION OF THE TEMPERATURE OF THE BOUNDARIES

B. G. Petrazhitskii and N. M. Stankevich

UDC 536.25

Many studies have examined natural convection in a horizontal cylinder. Nonsteady natural convection in closed rectangular and spherical cavities was examined in [1, 2]. A survey of different studies can be found in [3], while the latest publications are discussed in [4]. Some of these investigations consider the effect of a nonuniform distribution of the temperature of the boundaries. In particular, Gershuni et al. [5] and Ostrakh et al. [6] used approximate analytical methods to obtain information on local and integral characteristics of the given phenomenon in a steady-state regime. The authors made several simplifying assumptions that limited the range of application of the results. Thus, the data in [5] was obtained in a boundary-layer approximation, while the data in [6] is valid only for large Prandtl numbers and for Grashof numbers on the order of unity. The range of phase angles corresponding to cosine distributions of boundary temperature $0 < \varphi < \pi/2$ (Fig. 1), except for the region of the points $\varphi = 0$ (heating from the side) and $\varphi = \pi/2$ (heating from below).

A numerical solution to the problem was described in [7] for $-\pi/2 < \varphi < \pi/2$. Extensive information was presented on the streamlines and isotherms for different φ and Pr = 1. In contrast to the present study, the results in [7] pertain only to the steady-state regime and contain no information on velocity and temperature fields or local heat-transfer characteristics.

We attempted to solve the complete system of Navier–Stokes equations by numerical methods to obtain data on the process of establishment of a steady-regime and fill in the missing data for it for the range $10^4 < Ra < 10^7$ and Pr = 0.68 (helium) at $-\pi/2 < \varphi \leq 0$.

The given phenomenon has several important practical applications and is described by the system of equations of motion, continuity, and energy. We will study the two-dimensional laminar flow of an incompressible fluid with constant physical properties and a linear temperature dependence of density. After we exclude pressure and introduce the stream function ψ, this system takes the following form in polar coordinates (r, θ) for the conditions of the given problem (ω is curl and Φ is temperature):

Gorky. Translated from Zhurnal Prikladnoi Mekhaniki i Tekhnicheskoi Fiziki, No. 1, pp. 71-77, January-February, 1991. Original article submitted January 23, 1988; revision submitted June 26, 1989.

0021-8944/91/3201-0067$12.50

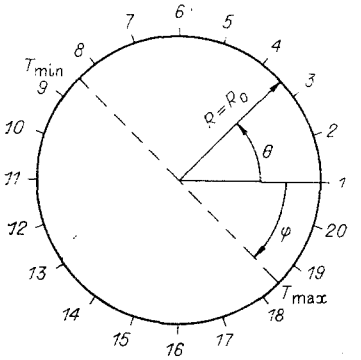

Fig. 1

$$\frac{\partial\omega}{\partial\tau}=\frac{1}{r}\left(\frac{\partial\psi}{\partial r}\frac{\partial}{\partial\theta}-\frac{\partial\psi}{\partial\theta}\frac{\partial}{\partial r}\right)\omega-\frac{1}{\mathrm{Gr}}\left(\frac{\partial}{\partial r}\cos\theta-\frac{\sin\theta}{r}\frac{\partial}{\partial\theta}\right)\Phi+\frac{1}{\mathrm{Gr}}\left(\frac{\partial^2}{\partial r^2}+\frac{1}{r}\frac{\partial}{\partial r}+\frac{1}{r^2}\frac{\partial^2}{\partial\theta^2}\right)\omega; \tag{1}$$

$$\left(\frac{\partial^2}{\partial r^2}+\frac{1}{r}\frac{\partial}{\partial r}+\frac{1}{r^2}\frac{\partial^2}{\partial\theta^2}\right)\psi=\omega; \tag{2}$$

$$\frac{\partial\Phi}{\partial\tau}=\frac{1}{r}\left(\frac{\partial\psi}{\partial r}\frac{\partial}{\partial\theta}-\frac{\partial\psi}{\partial\theta}\frac{\partial}{\partial r}\right)\Phi+\frac{1}{\mathrm{Ra}}\left(\frac{\partial^2}{\partial r^2}+\frac{1}{r}\frac{\partial}{\partial r}+\frac{1}{r^2}\frac{\partial^2}{\partial\theta^2}\right)\Phi, \tag{3}$$

where the components of the velocity vector are connected with the stream function by the relations $v_r=\frac{1}{r}\frac{\partial\psi}{\partial\theta}$, $v_\theta=-\frac{\partial\psi}{\partial r}$. We used the following scales to reduce (1)-(3) to dimensionless form: $\nu\mathrm{Gr}$) stream function; $\nu\mathrm{Gr}/R_0^2$) curl; $\nu\mathrm{Gr}/R_0$) velocity; $R_0^2/\nu\mathrm{Gr}$) time; R_0) linear dimensions (R_0 is the radius of a cylindrical cavity – see Fig. 1); $\mathrm{Gr}=gR_0^3\beta\Delta T/\nu^2$ is the Grashof number; $\mathrm{Pr}=\nu/a$ is the Prandtl number; $\mathrm{Ra}=\mathrm{GrPr}$ is the Rayleigh number; $\Phi=(T-T_0)/\Delta T$ is temperature; $\Delta T=(T_{max}-T_{min})/2$, $T_0=(T_{max}+T_{min})/2$.

The boundary conditions for the system of equations satisfy the requirement of impermeability of the boundaries and the adhesion conditions: $\partial\psi/\partial r=\partial\psi/\partial\theta=0$ at $r=1$. The temperature of the boundaries changed in accordance with the law $\Phi=\cos(\theta+\varphi)$ at $r=1$, where φ is the phase angle (see Fig. 1) corresponding to the maximum temperature on the inside surface of the cylinder. Approximately the same temperature distribution over the surface of a container is seen, for example, in the heating of a balloon by the sun.

We assumed that the fluid (gas) was initially in a state of mechanical equilibrium and that its temperature was equal to zero. We also studied the processes involved in establishment of a steady state. As the initial data for these processes, we used the fields of ψ, ω, and Φ obtained in previous computing variants (with lower Ra or other φ).

To solve system (1)-(3), we chose its finite-difference analog

$$\frac{\omega_{i,j}^{n+1}-\omega_{i,j}^{n}}{\Delta\tau}=\frac{1}{r_i}\left(\frac{\delta\psi^n}{\delta r}\frac{\delta\omega^n}{\delta\theta}-\frac{\delta\psi^n}{\delta\theta}\frac{\delta\omega}{\delta r}\right)-\frac{1}{\mathrm{Gr}}\left(\frac{\delta\Phi^n}{\delta r}\cos\theta_j-\frac{\sin\theta_j}{r_i}\frac{\delta\Phi^n}{\delta\theta}\right)+\frac{1}{\mathrm{Gr}}\left(\frac{\delta^2\omega^n}{\delta r^2}+\frac{1}{r_i}\frac{\delta\omega^n}{\delta r}+\frac{1}{r_i^2}\frac{\delta^2\omega^n}{\delta\theta^2}\right); \tag{4}$$

$$\frac{\left(\psi_{i,j}^{n+1}\right)^{k+1/2}-\left(\psi_{i,j}^{n+1}\right)^{k}}{0{,}5\sigma}=\frac{\delta^2(\psi^{n+1})^{k+1/2}}{\delta r^2}+\frac{1}{r_i}\frac{\delta(\psi^{n+1})^{k+1/2}}{2\delta r}+\frac{1}{r_i^2}\frac{\delta^2(\psi^{n+1})^{k}}{\delta\theta^2}-\omega_{i,j}^{n+1},$$

$$\frac{\left(\psi_{i,j}^{n+1}\right)^{k+1}-\left(\psi_{i,j}^{n+1}\right)^{k+1/2}}{0.5\sigma}=\frac{\delta^2(\psi^{n+1})^{k+1/2}}{\delta r^2}+\frac{1}{r_i}\frac{\delta(\psi^{n+1})^{k+1/2}}{2\delta r}+\frac{1}{r_i^2}\frac{\delta^2(\psi^{n+1})^{k+1}}{\delta\theta^2}-\omega_{i,j}^{n+1}; \tag{5}$$

$$\frac{\Phi_{i,j}^{n+1}-\Phi_{i,j}^{n}}{\Delta\tau}=\frac{1}{r_i}\left(\frac{\delta\psi^{n+1}}{\delta r}\frac{\delta\Phi^n}{\delta\theta}-\frac{\delta\psi^{n+1}}{\delta\theta}\frac{\delta\Phi^n}{\delta r}\right)+\frac{1}{\mathrm{Ra}}\left(\frac{\delta^2\Phi^n}{\delta r^2}+\frac{1}{r_i}\frac{\delta\Phi^n}{\delta r}+\frac{1}{r_i^2}\frac{\delta^2\Phi^n}{\delta\theta^2}\right), \tag{6}$$

where the difference operators

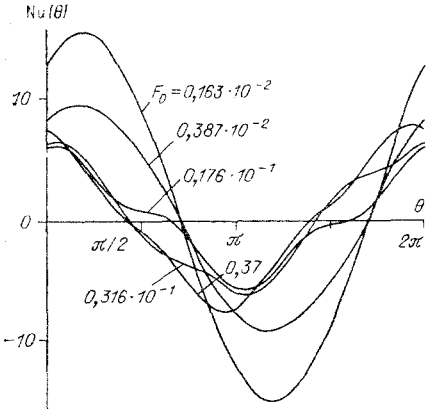

Fig. 2

$$\frac{\delta f}{\delta r} = \frac{f_{i+1,j} - f_{i-1,j}}{2\Delta r}; \quad \frac{\delta^2 f}{\delta r^2} = \frac{f_{i+1,j} - 2f_{i,j} + f_{i-1,j}}{\Delta r^2}; \quad \frac{\delta f}{\delta \theta} = \frac{f_{i,j+1} - f_{i,j-1}}{2\Delta\theta};$$

$$\delta^2 f/\delta\theta^2 = (f_{i,j+1} - 2f_{i,j} + f_{i,j-1})/\Delta\theta^2.$$

The procedure used to calculate the unknown functions is as follows. Using the known values of $\Phi_{i,j}{}^n$, $\omega_{i,j}{}^n$, $\psi_{i,j}{}^n$, we determine $\omega_{i,j}{}^{n+1}$ from (4). Then using the difference scheme for the direction variables (5) for each time layer, we find $\psi_{i,j}{}^{n+1}$ by the method of iteration (where σ is the iteration parameter). At the boundary nodes $\omega_{N,j}{}^{n+1} = \frac{8\psi_{N-1,j}^{n+1} - \psi_{N-2,j}^{n+1}}{2\Delta r^2}$, where N is the number of nodes along the coordinate r. In accordance with (6), with allowance for the boundary conditions we obtain $\Phi_{i,j}{}^{n+1}$. At the point r = 0, $f_{1,j}{}^{n+1} = \frac{1}{M}\sum_{j=1}^{M} f_{2,j}^{n+1}$. The cycle is then repeated. Calculations were performed on grids with the dimensions 21 × 21, 21 × 41, and 41 × 41. The main series of solutions was obtained on a 21 × 21 grid.

Let us examine the laws governing the development of natural convection at $\varphi = -\pi/5$ and Ra = 44,640. An analysis of the solutions shows that the process of establishment of a steady state can be broken down into three stages. At $F_0 \lesssim 0.6 \cdot 10^{-2}$, we have the initial stage, with the effect of heat conduction being dominant. This is indicated by the cosine distribution law for the Nusselt numbers $Nu(\theta) = (\partial\Phi/\partial r)_{r=1} = q_{st}R_0/\lambda\Delta T$ along the boundaries of the container. That convection is neligible at this stage and can be inferred from the coincidence of the angular positions of the extreme values of Nu and the positions of Φ_{max} and Φ_{min} given in the boundary conditions (Fig. 2). The family of curves $Nu(\theta)$ constructed for $F_0 = a\tau_1/R_0{}^2$ [curve 1) $F = 0.163 \cdot 10^{-2}$; 2) $0.387 \cdot 10^{-2}$; 3) $0.176 \cdot 10^{-1}$; 4) $0.316 \cdot 10^{-1}$; 5) 0.37] shows that the decrease in the Nusselt numbers with an increase in F_0 is slowed, while the points corresponding to heat flux $q_{st} = 0$ at this stage remain nearly stationary along the boundary over time. For example, the numbers $F_0 = 0.79 \cdot 10^{-3}$; $0.27 \cdot 10^{-2}$; $0.64 \cdot 10^{-2}$ correspond to the values $Nu_{max} = 20.6$; 11.5; 7.1. As it is heated, the fluid moves along the boundaries of the container in the counterclockwise direction, forming a slow-moving core (with $r < 0.825$, $v_\theta < 0.5 \cdot 10^{-4}$) with a complex two-vortex flow structure in the central part. The streamlines near the boundaries are close to being circles. The tangential component of velocity v_θ is directed counterclockwise. With a decrease in radius, the streamlines deviate from the center in diametrically opposite directions in the form of a figure eight, and vortex structures with a counterclockwise rotation are formed in the loops of this figure. The centers of the vortices are located at the ends of a diameter inclined to the horizontal at an angle $\theta \approx 22°$ with $F_0 = 0.6 \cdot 10^{-2}$. The temperature of the fluid changes significantly only near the walls (the upper left quadrant in Fig. 3, $F_0 = 0.387 \cdot 10^{-2}$). The enumeration of the profiles of $\Phi(r)$ and $v_\theta(r)$ in Figs. 3 and 4 correspond to the angular marking in Fig. 1. At $r < 0.8$, the isothermal region with the temperature $\Phi = 0$ remains intact.

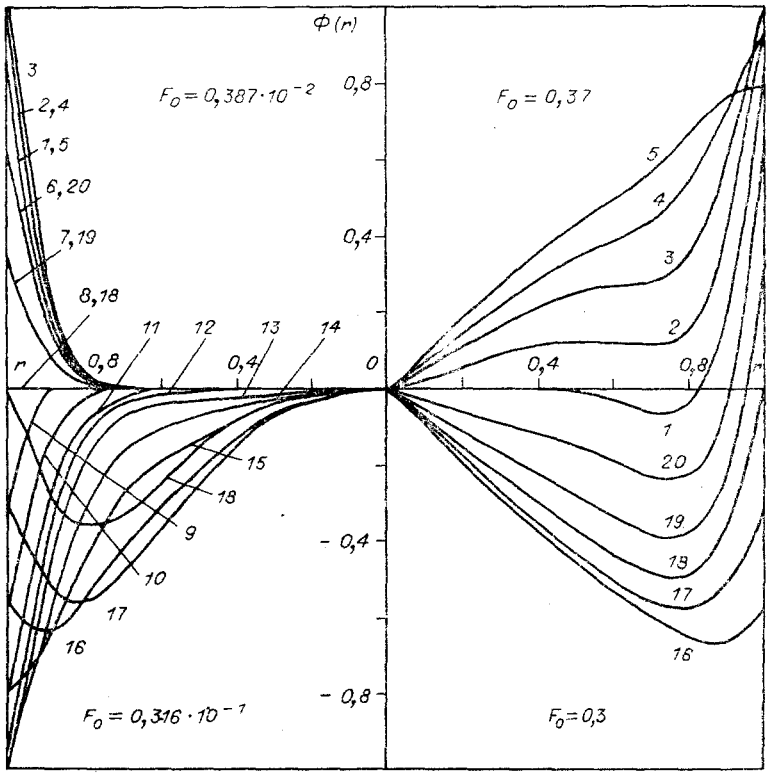

Fig. 3

The temperature and velocity profiles corresponding to the same given diameter are characterized by inverse symmetry relative to the coordinate origin (r = 0). This property remains in later stages of the heat-transfer process. Using it for the family of profiles of temperature $\Phi(r)$ and velocity $v_\theta(r)$ shown in Figs. 3 and 4 for different θ and F_0, we can construct profiles for the other half of the cylinder.

The second, transitional stage begins at $0.6 \cdot 10^{-2} < F_0 < 0.15$ and is characterized by intensive development of convection in the cavity and restructuring of the velocity and temperature fields. Over time the level of velocities v_θ rapidly rises throughout the region, including the previously slow-moving central zone. The action of the field of external body forces causes the convective flow near the boundaries to be directed upward along the heated wall and downward along the cold wall. In the initial stage, the streamlines are bunched in the boundary layer, with the angles $\theta \approx \pi/10$ and $11\pi/10$, $0.85 < r < 0.95$. Then as velocity level increases, the region of highest streamline density and, thus, greatest flow rate shifts in the direction of the flow. The velocity profiles $v_\theta(r)$ are different for each polar angle θ and have extrema. At each moment of time, for $v_{\theta max}$ in the flow field there is a certain angle $\theta = \theta_{max}$ at which it gradually increases with an increase in F_0 in the first stage, beginning from $\theta_{max} \approx \pi/10$. The value of θ_{max} increases in the second stage, reaching its highest value $\pi/4$ at $F_0 \approx 0.025$. It decreases at $F_0 \geq 0.025$ and approaches zero by the end of the stage. In particular, at $F_0 = 0.275 \cdot 10^{-2}$ $v_{\theta max} = 0.29 \cdot 10^{-3}$, $\theta_{max} = \pi/10$, while at $F_0 = 0.176 \cdot 10^{-1}$ $v_{\theta max} = 0.143 \cdot 10^{-2}$, $\theta_{max} \approx 2\pi/10$. The highest value $v_{\theta max} = 0.164 \cdot 10^{-2}$ is reached at $F_0 = 0.025$. The character of the velocity profiles $v_\theta(r)$ constructed for different F_0 shows that in the third stage the largest change in the structure of the velocity field occurs in the central part of the cylinder, rather than near the wall.

Figure 5 shows the streamlines and isotherms obtained at Ra = 44,640, $\varphi = -\pi/5$, $F_0 = 0.0316$, corresponding to the second stage of the process of establishment of a steady state. The penetration of the colder zones by the heated boundary layers of fluid and vice versa is evident on the isotherms for different F_0. In the second stage, the lines of the isotherms in the boundary region take the form of projections directed the same as the flow. On the temperature profiles, this is evident from the points of inflection on the curves and, later, the extrema at certain θ (see Fig. 3, $F_0 = 0.316 \cdot 10^{-1}$, $F_0 = 0.37$).

The motion of the layers of liquid relative to the wall leads to a shift in the extreme values of Nu in the counterclockwise direction (see Fig. 2) for $F_0 > 0.387 \cdot 10^{-2}$ (second

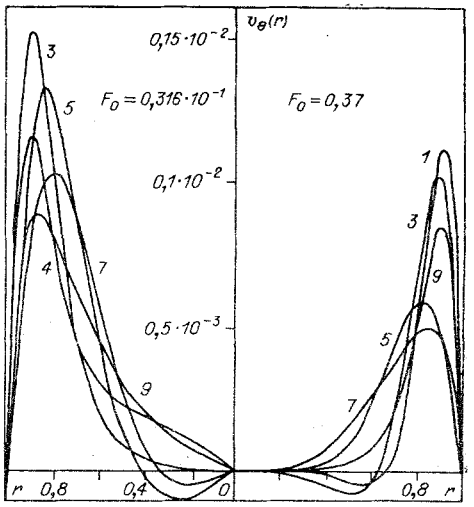

Fig. 4

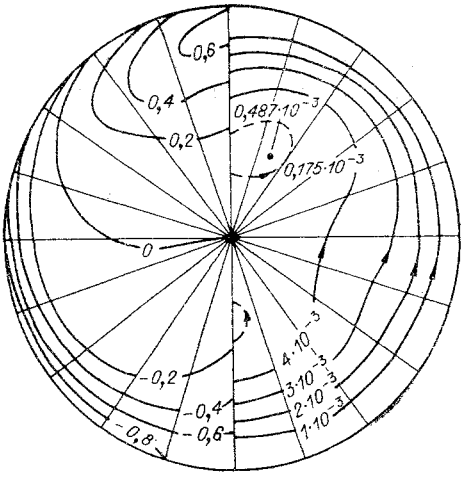

Fig. 5

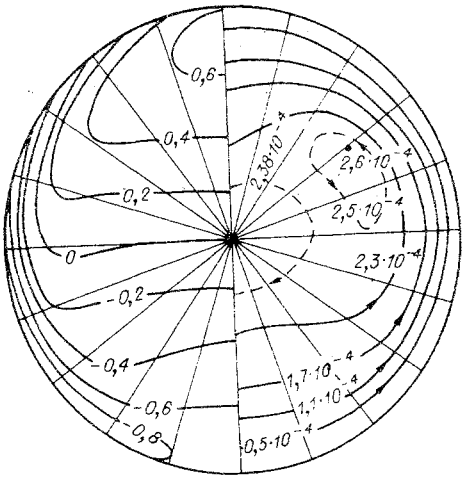

Fig. 6

stage of the process). The heated region, rising along the wall, reduces $(\partial\Phi/\partial r)_{r=1}$. Conversely, the downstream regions help increase $(\partial\Phi/\partial r)_{r=1}$ as they are induced to move. It is evident from the change in the temperature profiles and the isotherms that the temperature field in the boundary layer has for the most part already been formed by the beginning of the second stage, while the formation of the structure of the temperature field in the core continues until a steady-state regime has been completely established. This feature of the establishment process is reflected in the character of the distribution of $Nu(\theta)$ along the boundaries of the cylinder. The formation of the temperature field in the boundary layer is accompanied by the assumption of more or less stable positions by the extrema $Nu_{max}(\theta)$, $Nu_{min}(\theta)$ with respect to both phase and amplitude at $F_0 \gtrsim 0.9\cdot10^{-2}$. Later, as a stratified temperature field is formed in the central region as a result of thermal interaction of this region and the periphery, characteristic steps appear on the curves $Nu(\theta)$. Over time, these steps are displaced in the direction of the flow and ultimately merge with the extrema (see Fig. 2, $F_0 \geq 0.176\cdot10^{-1}$).

The formation of the internal structure of the flow is nearly complete by the end of the third stage $F_0 \gtrsim 0.15$. There is almost no change in the velocity and temperature fields over time. A slow-moving core with a characteristic vertical temperature stratification is formed in the central part of the cylinder ($r < 0.6$). The largest temperature gradients at the boundaries $(\partial\Phi/\partial r)_{r=1}$ and, thus, the most extreme values of $Nu(\theta)$ relative to the first stage are phase-shifted counter to the flow by the angle $\approx 48°$. The curve $Nu(\theta)$ is close to a sinusoid. The velocity profiles $v_\theta(r)$ have extrema near the boundaries at $0.8 < r < 0.9$. As in the first stage, in the steady-state regime the largest value $v_{\theta max}$ corresponds to

TABLE 1

Ra	$\Delta\theta=\lvert\varphi+\theta_{max}\rvert$, deg		
	$\varphi=0$	$\varphi=-\pi/5$	$\varphi=-2\pi/5$
$0{,}446\cdot10^5$	27	47,7	63,5
$0.446\cdot10^6$	30.6	52.5	70.2

$\theta_{max} \approx \pi/10$ (see Fig. 4, $F_0 = 0.37$). At $F_0 > 0.2$ a weak ellipsoidal eddy appears in the central part of the region. This eddy rotates slowly in the clockwise direction (Fig. 6, $F_0 = 0.37$, $\varphi = -\pi/5$, Ra = 44,640).

The characteristic signs of all of the stages of restructuring of the flow with zero initial conditions turned out to be the same for the range of phase angles $-\pi/5 \leq \varphi \leq 0$. In the case when the process of establishment of the steady-state regime begins from a state of hydrodynamic equilibrium corresponding to other values of Ra or φ, the fundamental laws remain the same only for the last two stages.

We analyzed the results of the numerical solution by the methods of the theory of similitude and dimensional theory. This analysis allowed us to obtain a generalized criterional formula to calculate the mean Nusselt numbers $\langle Nu\rangle$ at boundary nodes lying on a semicircle and corresponding to $q_{st}(\theta) = 0$. For the conditions of the steady-state regime, these numbers have the form $\langle Nu\rangle = cRa^n$, where $n = 0.0355\varphi + 0.3106$, $c = 0.1823 - 0.3\cdot10^{-4}\exp(-6.2577\varphi)$.

The position of Nu_{max} depends on Ra and φ. Table 1 shows values of $\Delta\theta = \lvert\varphi + \theta_{max}\rvert$ for certain solutions. The given criterional relation can be used at $10^4 < Ra < 10^7$ within the range $-\pi/2 < \varphi \leq 0$.

An analysis of the effect of the mesh of the grid on the solutions that were obtained shows that the greatest effect is seen with the selection of a small step for r, while choosing a small step for θ has less of an effect. The influence of the step of the difference grid with respect to the value of Nu_{max} can be judged on the basis of the following data (where N is the number of nodes for the coordinate r, M the number for θ, $Ra = 4.5\cdot10^5$, and $\varphi = 0$): $N \times M = 21 \times 21$, 21×41, 41×41, $Nu_{max} = 19.4$, 19.5, 16.6, respectively. Large differences in the distribution of the local $Nu(\theta)$ on different grids were seen only on relatively small sections of the boundaries: $\theta_{max} \pm \pi/10$ and $\theta_{min} \pm \pi/10$. An increase in the number of nodes for the coordinate r led to a decrease in $\lvert Nu(\theta)\rvert$.

LITERATURE CITED

1. V. I. Polezhaev, "Nonsteady laminar thermal convection in a closed region with a prescribed heat flux," Mekh. Zhidk. Gaza, No. 4 (1970).
2. E. L. Tarunin, "Nonsteady thermal convection in a spherical cavity," ibid., No. 4 (1970).
3. "Study of heat-transfer processes in structural elements," Tr. Mosk. Vyssh. Tekh. Uchil., No. 170 (1973).
4. O. G. Martynenko and Yu. A. Sokovishin, Free-Convective Heat and Mass Transfer: Bibliography [in Russian], ITMO Akad. Nauk Belorussian SSR, Minsk (1982-1987).
5. G. Z. Gershuni and E. M. Zhukhovitskii, "Closed convective boundary layer," Dokl. Akad. Nauk SSSR, 124, No. 2 (1959).
6. S. Ostrakh and E. R. Menold, "Natural convection inside a horizontal cylinder," in: Heat and Mass Transfer [in Russian], Vol. 1, Énergiya, Moscow (1968).
7. V. I. Chernatynskii, "Numerical study of convection in a horizontal cylinder of circular cross section," in: Hydrodynamics [in Russian], Vol. 7, Perm. Ped. Inst., Perm (1974).